J Inherit Metab Dis
DOI 10.1007/s10545-014-9676-9

ORIGINAL ARTICLE

Unravelling the complex MRI pattern in glutaric aciduria type I using statistical models—a cohort study in 180 patients

Sven F. Garbade · Cheryl R. Greenberg · Mübeccel Demirkol · Gülden Gökçay · Antonia Ribes · Jaume Campistol · Alberto B. Burlina · Peter Burgard · Stefan Kölker

Received: 16 July 2013 / Revised: 2 January 2014 / Accepted: 13 January 2014

Abstract
Background Glutaric aciduria type I (GA-I) is a cerebral organic aciduria caused by inherited deficiency of glutaryl-CoA dehydrogenase and is characterized biochemically by an accumulation of putatively neurotoxic dicarboxylic metabolites. The majority of untreated patients develops a complex movement disorder with predominant dystonia during age 3–36 months. Magnetic resonance imaging (MRI) studies have demonstrated striatal and extrastriatal abnormalities.
Aims/methods The major aim of this study was to elucidate the complex neuroradiological pattern of patients with GA-I and to associate the MRI findings with the severity of predominant neurological symptoms. In 180 patients, detailed information about the neurological presentation and brain region-specific MRI abnormalities were obtained via a standardized questionnaire.
Results Patients with a movement disorder had more often MRI abnormalities in putamen, caudate, cortex, ventricles and external CSF spaces than patients without or with minor neurological symptoms. Putaminal MRI changes and strongly dilated ventricles were identified as the most reliable predictors of a movement disorder. In contrast, abnormalities in globus pallidus were not clearly associated with a movement disorder. Caudate and putamen as well as cortex, ventricles and external CSF spaces clearly collocalized on a two-dimensional map demonstrating statistical similarity and suggesting the same underlying pathomechanism.
Conclusions This study demonstrates that complex statistical methods are useful to decipher the age-dependent and region-specific MRI patterns of rare neurometabolic diseases and that these methods are helpful to elucidate the clinical relevance of specific MRI findings.

Communicated by: Nicole Wolf

Electronic supplementary material The online version of this article (doi:10.1007/s10545-014-9676-9) contains supplementary material, which is available to authorized users.

S. F. Garbade
SFG: Faculty of Applied Psychology, SRH University of Applied Sciences, Heidelberg, Germany

S. F. Garbade · P. Burgard · S. Kölker (✉)
Department of General Pediatrics, Division of Inherited Metabolic Diseases, University Children's Hospital Heidelberg, Im Neuenheimer Feld 430, 69120 Heidelberg, Germany
e-mail: stefan.koelker@med.uni-heidelberg.de

C. R. Greenberg
Department of Biochemistry and Medical Genetics, Winnipeg Children's Hospital, University of Manitoba, Winnipeg, MB, Canada

M. Demirkol · G. Gökçay
Department of Nutrition and Metabolism, Children's Hospital, Istanbul Medical Faculty, Istanbul, Turkey

A. Ribes
Division of Inborn Errors of Metabolism, Department of Biochemistry and Molecular Genetics, Hospital Clinic and CIBERER, Barcelona, Spain

J. Campistol
Neuropediatrics Service, Hospital Sant Joan de Deu, Barcelona, Spain

A. B. Burlina
University Children's Hospital, Padova, Italy

Published online: 09 May 2014

Abbreviations

FLAIR	Fluid attenuated inversion recovery
GA-I	Glutaric aciduria type I (OMIM #231670)
MD	Movement disorder
MDS	Multi-dimensional scaling
MRI	Magnetic resonance imaging

Introduction

Glutaric aciduria type I (GA-I; OMIM #231670) is caused by autosomal recessive deficiency of the mitochondrial flavoprotein glutaryl-CoA dehydrogenase (EC 1.3.99.7) which catalyzes the oxidative decarboxylation of glutaryl-CoA within the final degradative pathway of L-lysine, L-hydroxylysine, and L-tryptophan (Goodman et al 1975). This homotetrameric enzyme is encoded by the *GCDH* gene localized on 19p13.2. More than 200 disease-causing mutations have so far been identified (Busquets et al 2000; Zschocke et al 2000). The biochemical hallmark of this disease is accumulation of putatively neurotoxic glutaryl-CoA, glutaric acid, and 3-hydroxyglutaric acid as well as non-toxic glutarylcarnitine (Sauer et al 2005; Lamp et al 2011). Cerebral entrapment of these dicarboxylic metabolites is the consequence of their inefficacious efflux transport across the blood–brain barrier (Kölker et al 2006a, b; Sauer et al 2010).

The majority of untreated patients during age 3–36 months develop a complex extrapyramidal syndrome with predominant dystonia (Gitiaux et al 2008; Kölker et al 2006a, b) which may manifest acutely during an encephalopathic crisis or insidiously over weeks and months (Kölker et al 2007; Heringer et al 2010). A neuroradiological study using magnetic resonance imaging (MRI) has provided evidence that acute and insidious onset of dystonia is induced by a similar mechanism but differs with regard to the timing of striatal injury (Strauss et al 2007). Striatal injury can be prevented in the majority of patients identified by newborn screening if they follow evidence-based treatment recommendations which consist of low lysine diet, carnitine supplementation and emergency treatment during episodes that are likely to induce catabolism (Heringer et al 2010; Kölker et al 2011). The positive effect of newborn screening and metabolic treatment on the neurological outcome has been confirmed in various newborn screening cohorts worldwide (Kölker et al 2007; Strauss et al 2007; Bijarnia et al 2008; Boneh et al 2008; Viau et al 2012; Couce et al 2013), and the cost-effective of newborn screening for GA-I has recently been demonstrated (Pfeil et al 2013). Metabolic treatment aims to limit the accumulation of neurotoxic dicarboxylic metabolites in the brain. Recently, biochemical proof of principle has been provided for this metabolic treatment in Gcdh-deficient mice (Zinnanti et al 2007; Sauer et al 2011).

Previous neuroradiological studies have mostly focused on symptomatic GA-I patients (Neumaier-Probst et al 2004; Strauss et al 2007). Growing evidence, however, points to a more complex age-dependent and region-specific MRI phenotype which may also affect clinically asymptomatic patients (Twomey et al 2003; Külkens et al 2005; Harting et al 2009). This includes MRI abnormalities of white matter and extrastriatal grey matter such as in globus pallidus. In addition, some MRI abnormalities such as temporal hypoplasia are already found in newborns suggesting intrauterine neuropathology (Lin et al 2002; Harting et al 2009). The clinical relevance and long-term prognosis of these MRI findings remains to be elucidated.

The aim of this study is to investigate the complex pattern of grey and white matter MRI abnormalities in specific brain regions of patients with GA-I. Specifically, we investigated the correlation of MRI changes with the severity of neurological symptoms and visualized similarities and dissimilarities of region-specific MRI findings using complex statistical methods.

Patients and methods

The major aim of this study was to elucidate the pattern of MRI abnormalities in a large cohort of patients with GA-I. A previous study has hypothesized that region-specific MRI abnormalities manifest at specific ages and that they may regress (e.g. temporal hypoplasia), may be stable for years (e.g. striatal lesions), or may progress (e.g. white matter changes) (Harting et al 2009). Therefore, we aimed to investigate whether MRI changes of specific brain regions were associated with each other and whether MRI changes correlated with the clinical phenotype.

Questionnaire-based survey

To test this, we used a questionnaire-based survey on the region-specific MRI findings and the neurological outcome in patients with GA-I—in analogy to a previous cross-sectional study (Kölker et al 2006a, b). Patients with unconfirmed diagnosis or with glutaric aciduria type II and III were excluded. The study was approved by the institutional ethics committee of the University of Heidelberg (No. 314/2002 and S-049/2010), and patient data were only included if written informed consent was obtained from patients and/or their parents. Patients were pseudonymized and double entries were excluded by birthdate and gender. Finally, questionnaires from 180 patients were included into the statistical analysis. Clinical, diagnostic and therapeutic data of 157 of these patients have been reported previously (Kölker et al 2006a, b). All patient-related information (e.g. chronological age, MRI study, neurological examination) referred to the date of a

single study visit. We have not used a follow-up design with multiple visits and serial MRI studies.

Neurological examination and assessment of the severity of a movement disorder (if any) as well as region-specific analysis of MRI findings of study patients according to a predefined rating schedule were performed by all contributing centres independently. Results were filled in a questionnaire and returned to the coordinating centre (University Children's Hospital, Heidelberg). Validation of neuroradiological and neurological findings was not performed using a multi-rater design in a blinded manner. Therefore, inter-observer reliability of this dataset is unknown. However, the rating schedule used in this study has been evaluated in a previous study by three independent raters in a blinded manner (Harting et al 2009). Inter-observer realibility (expressed a Fleiss' κ) using a dichotomized design was found to be almost perfect for putamen (0.93), globus pallidus (0.93) and caudate (0.85), substantial for white matter changes (0.61), moderate for subdural hematoma/hygroma (0.49), thalamus (0.48), (frontal) external CSF spaces (0.44), fair for cerebellum (0.31), and slight for cortex (0.13).

Assessment of the neurological outcome

To evaluate the neurological outcome we determined the severity of the complex movement disorder (MD) and the morbidity score as previously described (Kölker et al 2006a, b, 2007; Heringer et al 2010). The severity of MD was estimated by caring physicians (0 point = unaffected; 1 point = slight [i.e. MD not causing disability in daily life]; 2 points = mild [i.e. MD without significant disability in daily life]; 3 points = moderate [i.e. MD that interferes with normal posturing and/or functional activities of the upper and/or lower extremities]; 4 points = severe [i.e. limiting generalized MD that prevents normal position and significantly restricts the functional activites of the upper and lower extremities]). Morbidity was assessed using a sum score of four items (0 point = no, 1 point = yes; for each item) ranging from 0 points (asymptomatic) to 4 points (severe morbidity). Single items included in this score were (1) loss of mobility, (2) feeding problems such as difficulties with swallowing and the necessity of tube feeding, (3) respiratory problems such as recurrent (aspiration) pneumonia, and (4) epilepsy requiring treatment. MD and morbidity scores have been defined in advance.

Assessment of MRI findings

Neuroradiological findings were evaluated by MRI (T1w, T2w, and fluid attenuated inversion recovery [FLAIR] images). The following regions and abnormalities were assessed as follows: (1) cortex (0=unaffected, 1=temporal hypoplasia or atrophy, 2=frontal and temporal hypoplasia or atrophy), (2) putamen, (3) caudate, (4) globus pallidus, (5) thalamus, (6) cerebellum (for regions 2–6: 0=unaffected, 1=T2 hyperintensity, 2=atrophy), (7) white matter (0=unaffected, 1=localized T2 hyperintensity, 2=generalized or diffuse T2 hyperintensity), (8) subdural hematoma/hygroma (0=none, 1=unilateral, 2=bilateral), (9) ventricles (0=unaffected, 1=mildly or moderately dilated, 2=strongly dilated), and (10) external CSF spaces (0=unaffected, 1=mildly or moderately dilated, 2=strongly dilated). For systematic reasons we also included brain regions which are not thought to be affected in GA-I.

A previous study has elucidated that putatively reversible temporal hypoplasia is frequently found in newborns with GA-I and that frontal and temporal atrophy may develop in addition after the manifestation of acute encephalopathic crises (Harting et al 2009). Since we used a single visit design, cortical volume deficits could not be clearly differentiated as hypoplasia or atrophy. Therefore, the questionnaire contains the term "hypoplasia or atrophy". In contrast to this, volume deficits of all other brain regions were thought to reflect atrophy, since previous studies have not provided evidence for hypoplasia of non-cortical brain regions (Twomey et al 2003; Strauss et al 2007; Harting et al 2009).

Statistical analysis

Statistical analysis was based on detailed information of returned questionnaires. Only questionnaires with a complete set of required neurological and neuroradiological data (n=180) were included in the statistical analysis. To investigate the relation between MRI abnormalities and the severity of motor dysfunction and morbidity, we used Kruskal Wallis test and subsequent Benjamini Hochberg correction of p values (Benjamini and Hochberg 1995). Tree-based classification method (Hothorn et al 2006) was used to determine parameters predicting the categorical outcome variables severity of MD and morbidity score. We used the implementation in the so-called ctree-function (Hothorn et al 2006). The analysis included independent variables of the neuroradiological evaluation of ten brain regions as described above. Multidimensional scaling (MDS) was used to explore the MRI pattern, i.e. the concomitant occurrence of neuroradiological changes in different brain regions. The MDS was computed in four steps: First, all tested neuroradiological items were correlated against each other using rank-based tau correlation coefficient. Second, a proximity matrix using Euclidean distances was computed from the correlation matrix of region-specific neuroradiological assessment. Third, the proximity matrix was represented by a two-dimensional map using non-metric multidimensional scaling implemented by Venables and Ripley (2002) for R and S. The scaling procedure aims to visualize similarities and dissimilarities of region-specific neuroradiological findings in patients with GA-I. A short distance of specific brain regions on the two-

dimensional map is thought to demonstrate statistical similarity of neuroradiological findings in these brain regions, whereas a large distance reflects dissimilarity. Fourth, to identify possible distortions in the MDS solution, a minimum-spanning tree was computed and plotted onto the two dimensional representation using the method of Paradis et al (2004). Potential distortions by the scaling solution are indicated when nearby points on the plot are not linked by an edge of the minimum-spanning tree.

To evaluate age-dependent effects of the MRI pattern, we performed MDS in all patients and compared them with the MDS of patients who were older than 3 years. Due to the small group size of patients under 3 years of age (n=27), MDS of this age group was not performed. Our methodological approach allows to identify an evolving MRI pattern, the association of region-specific MRI changes as well as the correlation between the neuroradiological and the clinical phenotype in a cohort of patients at different ages. In addition, we evaluated the frequency of region-specific MRI findings in four different age groups, i.e. ≤ 3 years, > 3 to≤10 years, > 10 to≤20 years, and>20 to 30 years. The analysis was not extended beyond 30 years of age, since only three patients (age 34, 41, and 67 years) were included in this age group. All statistical analyses and graphics were computed with R environment for statistical computing (R Development Core Team 2012).

Results

Study population

We included 180 patients (73 female, 107 male) with confirmed GA-I and complete information on MRI findings and neurological outcome parameters. Among them, 130 patients were neurologically symptomatic presenting with a complex MD with predominant dystonia superimposed on axial hypotonia, whereas 50 neonatally identified patients did show no or minor neurological symptoms. Neonatal diagnosis was made by extended newborn screening (n=21), high-risk family screening (n=18), high-risk population screening (n=2), or due to diagnostic work-up of macrocephaly (n=9). Diagnosis was confirmed by quantitative urinary organic acid analysis (all), *GCDH* gene analysis (n=116), and/or enzyme analysis (n=118). The mean chronical age as well as the age at study visit and MRI study was 10.2 years (standard deviation, 8.2 years; median, 9 years; range, 0.3–67.7 years) for all study patients. It was 10.1 years (standard deviation, 10 years; median, 7.2 years; range, 0.3–67.7 years) in symptomatic patients and 10.4 years (standard deviation: 6.8 years; median, 9.4 years; range, 0.5–39.4 years) in patients with no or minor symptoms. Ninety-sixth patients (53 % of all patients) were younger than 10 years, 27 of them were younger than 3 years of age and thus were in the vulnerable period for striatal injury, three of them were younger than 1 year. Sixty-eight patients (38 %) were between 10 and 20 years of age, 13 patients (7 %) between 20 and 30 years, and three patients (2 %) older than 30 years (Suppl. Figure 1).

At the time point of the study visit, 158 of 180 patients received a combination of low lysine diet with (n=91) or without (n=67) supplementation of lysine-free amino acid mixtures and carnitine supplementation for metabolic maintenance treatment. Sixteen patients received dietary treatment (n=6) or carnitine supplementation (n=10) alone, whereas six patients did not receive any metabolic treatment. Since the majority of study patients (88 %) received combined metabolic maintenance therapy, the impact of treatment on brain-specific MRI abnormalities could not be assessed.

Association of motor function and brain regions

First, we evaluated individual MRI findings with the neurological outcome evaluating morbidity score (Table 1) and the severity of MD (Table 2) using Kruskal Wallis test. Patients with a severe neurological phenotype which was dominated by a severe MD had more often MRI abnormalities in the cortex, putamen, caudate, ventricles and external CSF spaces and more often demonstrated subdural hematoma or hygroma than patients without or with minor neurological symptoms. Interestingly, MRI abnormalities of the globus pallidus, in particular T2 hyperintensity, were less clearly related with the neurological phenotype (morbidity score, p=0.049; severity of MD, p=0.051). No significant relation between the neurological phenotype and MRI abnormalities was found in thalamus, cerebellum, and white matter.

Since Kruskal Wallis analysis has identified five brain regions (i.e. cortex, putamen, caudate, ventricles and external CSF spaces) which were associated with the neurological phenotype of GA-I patients, we evaluated which of these brain regions and MRI abnormalities had the strongest effect on the neurological phenotype. For this purpose, we performed recursive partitioning since this statistical method can handle numerical data that are highly skewed or multimodal, as well as categorical predictors with either ordinal or nonordinal structure. Using the morbidity score (Fig. 1) and the severity of MD (Fig. 2) as dependent variables in this statistical model we showed that MRI changes of the putamen (T2 hyperintensity and atrophy) as well as strongly dilated ventricles were the best predictors of a severe neurological phenotype. Evaluating the correlation between MRI changes in ten different brain regions demonstrated that neuroradiological changes in putamen respectively caudate and ventricles were only slightly correlated (r^2=0.35 and 0.37, respectively; Table 3), and thus did not provide unambiguous evidence that dilation of ventricles can be explained exclusively by striatal atrophy. Strongest correlations were obtained for putamen and

Table 1 Association between the MRI pattern and the morbidity score

Brain region	Rating	*N*	Morbidity score (minimum, 0 point = asymptomatic; maximum, 4 points = severe morbidity)			Kruskal Wallis test
			Mean	SD	Median	
Cortex	Unaffected	23	0.61	0.94	0	**χ^2 (2)=24.9, p<0.001**
	Temporal hypoplasia or atrophy	49	0.92	1.13	0	
	Frontal and temporal hypoplasia or atrophy	107	1.73	1.23	2	
Putamen	Unaffected	65	0.46	0.81	0	**χ^2 (2)=58.8, p<0.001**
	T2 hyperintensity	59	1.69	1.13	2	
	Atrophy	55	2.07	1.17	2	
Caudate	Unaffected	85	0.67	0.97	0	**χ^2 (2)=54.4, p<0.001**
	T2 hyperintensity	57	1.81	1.16	2	
	Atrophy	37	2.27	1.07	2	
Pallidum	Unaffected	123	1.20	1.20	1	**χ^2 (2)=11.9, p=0.010**
	T2 hyperintensity	43	1.51	1.26	2	
	Atrophy	13	2.46	1.23	2	
Thalamus	Unaffected	173	1.38	1.25	1	χ^2 (2)=0.5, p=0.847
	T2 hyperintensity	6	1.00	1.25	0.5	
	Atrophy	0	NA	NA	NA	
Cerebellum	Unaffected	175	1.37	1.24	1.0	χ^2 (2)=0.2, p=0.875
	T2 hyperintensity	0	NA	NA	NA	
	Atrophy	4	1.25	1.89	0.5	
White matter	Unaffected	121	1.81	1.16	1	**χ^2 (2)=8.5, p=0.0144**
	Localized T2 hyperintensity	44	1.84	1.27	2	
	Generalized or diffuse T2 hyperintensity	14	1.43	1.55	1	
Subdural hematoma/hygroma	None	160	1.28	1.20	1.0	**χ^2 (2)=6.6, p=0.049**
	Unilateral	6	2.50	1.52	2.5	
	Bilateral	13	1.92	1.44	2.0	
Ventricles	Unaffected	105	1.04	1.14	1	**χ^2 (2)=30.4, p<0.001**
	Mildly or moderately dilated	55	1.49	1.20	1	
	Strongly dilated	19	2.79	0.85	3	
External CSF spaces	Unaffected	22	0.77	1.02	0	**χ^2 (2)=24.1, p<0.001**
	Mildly or moderately dilated	59	0.90	1.09	0	
	Strongly dilated	98	1.78	1.24	2	

Statistical analysis was performed using Kruskal-Wallis test with Benjamini-Hochberg correction of *p* values. Significant differences were highlighted using bold letters

Data for the calculation of the morbidity score were incomplete in one patient

NA not applicable

caudate (r^2=0.75) as well as for cortex and external CSF spaces (r^2=0.79; Table 3). Similar results were obtained in patients older than 3 years of age (Suppl. Table 1)

Assessment of the MRI pattern

To unravel the complex neuropathology of GA-I and to elucidate whether MRI changes of the studied brain regions were associated with each other, we determined MDS. Evaluation of the item-item similarities revealed a stress of 2.12 %. Next, a minimum-spanning tree was calculated to assign a location to each item in a two-dimensional space. It demonstrates that some items collocalize, i.e. (1) cortex, ventricles, and external CSF spaces, as well as (2) putamen and caudate. MRI changes of globus pallidus, however, were localized in an intermediate position between putamen/caudate and white matter. In contrast, cerebellum, thalamus, and subdural hematoma/hygroma showed a distant localization (Fig. 3). Distances on the two-dimensional map are thought to reflect similarities (if parameters collocalize) and dissimilarities (if they are distant) of brain regions regarding their neuropathological involvement in GA-I.

MDS analysis was repeated in a subgroup of patients older than 3 years of age. The result of this analysis was very similar to that of the whole study group. Collocalization of cortex/

Table 2 Association between the MRI pattern and the severity of movement disorder

Brain region	Rating	*N*	Severity of MD (minimum, 0=no MD; maximum, 4=severe MD)			Kruskal Wallis test
			Mean	SD	Median	
Cortex	Unaffected	23	0.61	0.94	0	**χ^2 (2)=22, p<0.001**
	Temporal hypoplasia or atrophy	49	0.92	1.13	0	
	Frontal and temporal hypoplasia or atrophy	108	1.73	1.23	2	
Putamen	Unaffected	65	0.74	1.00	0	**χ^2 (2)=76, p<0.001**
	T2 hyperintensity	60	2.30	0.96	2	
	Atrophy	55	2.69	0.98	3	
Caudate	Unaffected	86	1.04	1.14	1	**χ^2 (2)=65.4, p<0.001**
	T2 hyperintensity	57	2.42	0.98	2	
	Atrophy	37	2.86	0.86	3	
Pallidum	Unaffected	124	1.75	1.30	2	χ^2 (2)=6, p=0.051
	T2 hyperintensity	43	1.91	1.31	3	
	Atrophy	13	2.69	0.95	3	
Thalamus	Unaffected	174	1.86	1.30	2.0	χ^2 (2)=0.004, p=0.941
	T2 hyperintensity	6	1.83	1.47	1.5	
	Atrophy	0	NA	NA	NA	
Cerebellum	Unaffected	176	1.87	1.30	2	χ^2 (2)=0.8, p=0.805
	T2 hyperintensity	0	NA	NA	NA	
	Atrophy	4	1.25	1.50	1	
White matter	Unaffected	122	1.51	1.21	1	χ^2 (2)=3.3, p=0.188
	Localized T2 hyperintensity	44	1.86	1.17	2	
	Generalized or diffuse T2 hyperintensity	13	1.38	1.32	2	
Subdural hematoma/hygroma	None	161	1.78	1.26	2	**χ^2 (2)=7.6, p=0.044**
	Unilateral	6	3.17	1.17	3.5	
	Bilateral	13	2.23	1.48	3	
Ventricles	Unaffected	105	1.46	1.23	1	**χ^2 (2)=33.9, p<0.001**
	Mildly or moderately dilated	56	2.14	1.23	2	
	Strongly dilated	19	3.21	0.54	3	
External CSF spaces	Unaffected	22	1.32	1.04	1	**χ^2 (2)=27.1, p<0.001**
	Mildly or moderately dilated	59	1.29	1.34	1	
	Strongly dilated	99	2.31	1.15	2	

Statistical analysis was performed using Kruskal-Wallis test with Benjamini-Hochberg correction of p values. Significant differences were highlighted using bold letters. NA, not applicable

external CSF spaces/ventricles and putamen/caudate as well as the intermediate positive of the pallidum was analogous (Suppl. Fig. 2).

Age-dependent frequency of MRI abnormalities in different brain regions

To investigate whether MRI abnormalities and their severity was discrepant in different age groups we evaluated four age groups (e.g. ≤ 3 years, > 3 to≤10 years, > 10 to≤20 years, and>20 to 30 years). MRI changes in putamen (Suppl. Fig. 3) and caudate (Suppl. Fig. 4) remained stable after age 3 years confirming the previously described window of vulnerability of the striatum in GA-I. The frequency and severity of white matter changes on MRI increased from younger to older age groups (Suppl. Fig. 5). In contrast, MRI abnormalities in the pallidum remained quite stable (Suppl. Fig. 6). Some brain regions such as the thalamus showed a very low frequency (if at all) of MRI changes in all age groups (Suppl. Fig. 7).

Discussion

The aim of this study was to investigate the pattern of MRI changes in specific brain regions of GA-I patients. Specifically, we studied the correlation of MRI changes with the severity of neurological symptoms and visualized similarities and dissimilarities of region-specific MRI findings using complex statistical methods. The major findings of this study

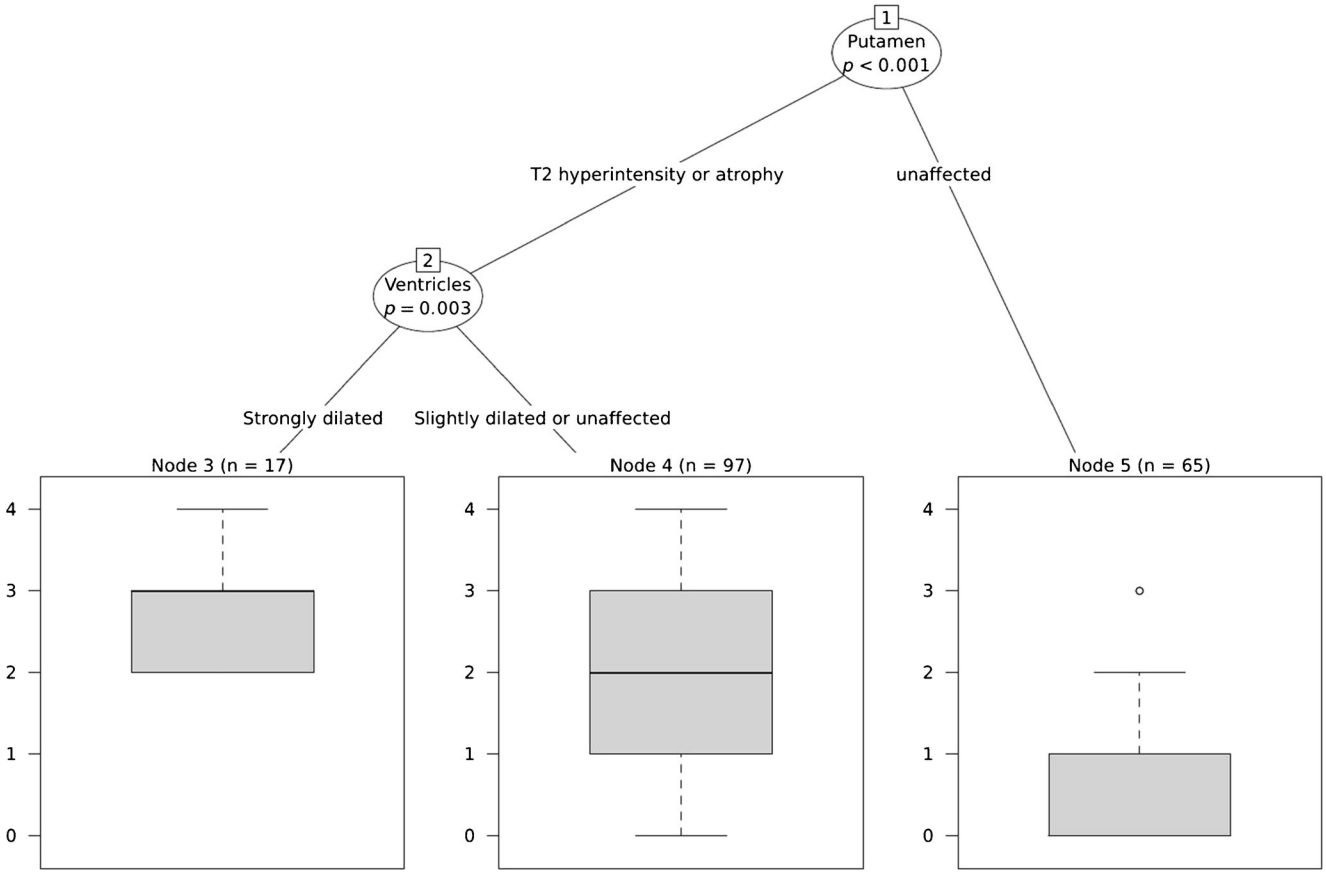

Fig. 1 Recursive partitioning model for region-specific MRI changes with morbidity score as dependent variable. The analysis demonstrates that a combination of MRI changes in the putamen (T2 hyperintensity or atrophy) plus strongly dilated ventricles are best neuroradiologic predictors for a poor neurologic outcome

in 180 patients are that (1) patients with a severe neurological phenotype due to a severe MD have more often MRI abnormalities in cortex, putamen, caudate, ventricles and external CSF spaces and more often demonstrate subdural hematoma or hygroma than patients without or with minor neurological symptoms; (2) T2 hyperintensity and atrophy of putamen as well as strongly dilated ventricles are the best predictors for a severe MD; (3) changes in white matter-rich globus pallidus are not clearly associated with a MD; (4) MRI abnormalities in i) cortex, ventricles, and external CSF spaces as well as in ii) putamen and caudate collocalize on a two-dimensional map, and (5) MRI changes in thalamus, cerebellum, and white matter are not associated with MD and do not collocolize. This study shows that a complex MRI pattern and its relevance for the clinical phenotype can be unravelled by complex statistical methods. Our results strongly support the notion of age-dependent and region-specific brain pathology involving both grey and white matter structures in GA-I patients. However, since a questionnaire-based study includes a risk of under- or overestimation of MRI changes, these results should be independently evaluated in a prospective study with repetitive MRI investigations and double blind analysis by two or more central raters.

Brain pathology of GA-I patients is complex and not yet fully understood (Funk et al 2005; Harting et al 2009). Toxic dicarboxylic metabolites which accumulate in the brain compartment due to very limited efflux transport of dicarboxylic acids across the blood–brain barrier are thought to impair cerebral energy metabolism via inhibition of 2-oxoglutarate dehydrogenase complex, the astrocyte-to-neuron dicarboxylic acid shuttle, and to facilitate excitotoxic cell damage specifically in striatal medium-spiny neurons (Sauer et al 2005, 2006, 2010; Zinnanti et al 2007; Lamp et al 2011). Toxic effects have also been demonstrated in immature oligodendrocytes (Gerstner et al 2005). In addition, disturbed autoregulation of cerebral perfusion was found in one MRI study; the mechanism remains to be elucidated (Strauss et al 2010). It has been speculated that age-dependent and region-specific mechanisms contribute to the manifestation of acute striatal injury (Zinnanti et al 2007). However, the above mentioned mechanisms would also favour the notion of chronic, life-long neurotoxicity in GA-I.

Whereas the manifestation of striatal injury—induced by acute encephalopathic crises or developing insidiously—is limited to a vulnerable period in infancy and childhood (i.e. usually between age 3–36 months), there is growing evidence

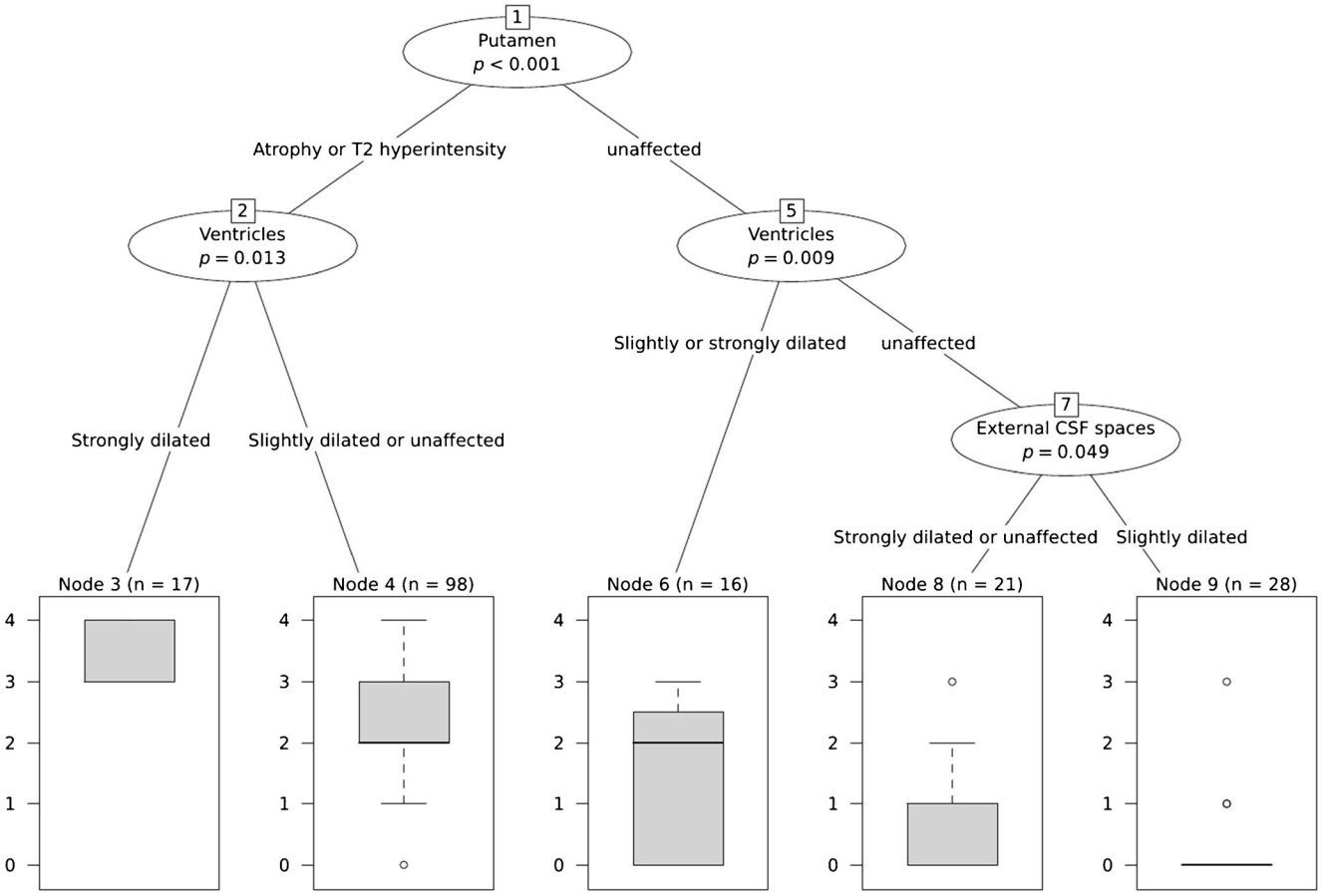

Fig. 2 Recursive partitioning model for region-specific MRI changes with severity of MD as dependent variable. The analysis demonstrates that a combination of MRI changes in the putamen (T2 hyperintensity or atrophy) plus strongly dilated ventricles are best neuroradiologic predictors for a poor neurologic outcome, whereas a combination of unaffected putamen plus unaffected ventricles was associated with the most favourable outcome

that extrastriatal pathology may already start in utero (Lin et al 2002; Harting et al 2009) and may slowly progress into adolescence and adulthood—with or without preceding striatal injury (Külkens et al 2005; Harting et al 2009). Temporal hypoplasia, widening of Sylvian fissures, immature gyral pattern, and delayed myelination are thought to reflect

Table 3 Correlations (r^2) between MRI changes

	Cortex	Putamen	Caudate	Pallidum	Thalamus	Cerebellum	White matter	Subdural hematoma/ hygroma	Ventricles	External CSF spaces
Cortex										
Putamen	0.38									
Caudate	0.41	**0.75**								
Pallidum	0.12	0.16	0.29							
Thalamus	0.04	0.09	0.02	0.02						
Cerebellum	0.05	0.01	−0.05	0.00	−0.03					
White matter	0.15	0.12	0.18	0.21	0.06	0.08				
Subdural hematoma/ hygroma	0.12	0.22	0.18	0.08	0.04	−0.05	−0.05			
Ventricles	0.42	0.35	0.37	−0.02	0.04	0.08	0.21	0.22		
External CSF spaces	**0.79**	0.43	0.40	0.11	0.11	0.07	0.25	0.18	0.44	

Strongest correlations were found between putamen and caudate as well as between cortex and external CSF spaces

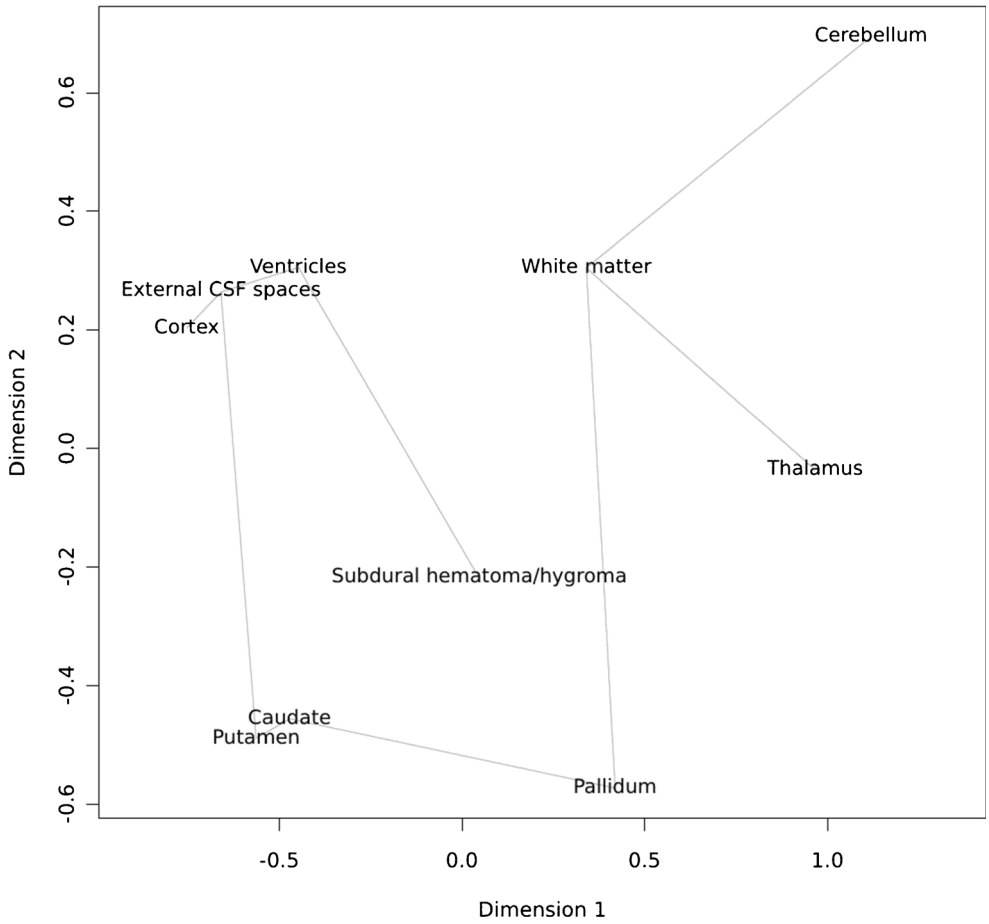

Fig. 3 Multidimensional scaling of neuroradiological items using the so-called minimum-spanning tree. The stress was 2.12 %. Collocalization of pathologic MRI changes in ventricles, external CSF spaces and cortex, as well as in caudate and putamen indicate similarities in the underlying mechanisms. Globus pallidus, a white-matter rich grey matter structure, is located between caudate/putamen and white matter indicating that pallidal MRI changes may reflect putatively reversible white matter pathology or irreversible basal ganglia damage

intrauterine pathology, whereas white matter signal abnormalities progress with age and usually spread from the periventricular to the deep white matter (Twomey et al 2003; Harting et al 2009).

The clinical relevance of intrauterine changes and late-onset white matter abnormalities remains to be elucidated, whereas the severity of striatal MRI changes has been correlated with the severity of the MD (Harting et al 2009). This is confirmed by our study showing that T2 hyperintensity and atrophy of putamen as well as strongly dilated ventricles are the best predictors of a severe MD. From a clinical point of view, an extrapyramidal MD would be expected in any disease with striatal lesions, whereas an association between MD and dilated ventricles requires further explanation. To our understanding, dilated ventricles in severely handicapped GA-I patients reflect *e vacuo* dilatation due to striatal atrophy and/or white matter pathology rather than impairment of CSF flux. Similarly, the slightly increased frequency of subdural hematomas in patients with a severe MD does not necessarily mean that subdural hematomas are space-occupying and thus deterioriate an MD. To our understanding, GA-I patients with a severe MD have more often cortical atrophy and dilated CSF spaces. This increases the risk of a mechanical trauma of brigding veins.

Although the MD of individual patients might be stable for years, it tends to progress from mobile to fixed dystonia and may be associated with akinetic-rigid parkinsonism, whereas muscular hypotonia tends to improve with aging (Gitiaux et al 2008). This progression may reflect the response of the developing brain to acute striatal damage in infancy. Alternatively, it may be explained by ongoing neuropathological changes in extrastriatal white and deep grey matter (Twomey et al 2003; Harting et al 2009). Although extrastriatal brain regions were not associated with the manifestation of MD in this study, these MRI changes might correlate with other clinical endpoints such as cognitive function, fine motor activity, language and reading skills, and processing speed—as it has been demonstrated for phenylketonuria (Janos et al 2012).

Whereas the striatal pathology and subsequent dystonia predominantly relies on the loss of striatal medium-spiny neurons and is thought to be (partially) induced by accumulating toxic dicarboxylic metabolites (Funk et al 2005), the white matter involvement in GA-I is less clear. Post mortem studies and investigations in Gcdh-deficient mice have provided evidence that the neuropathological correlate of MRI white matter changes is spongiform myelinopathy (Chow et al 1988; Soffer et al 1992). However, spongiform changes were also observed in grey matter regions (Chow et al 1988;

Zinnanti et al 2007). In GA-I patients, spongiform myelinopathy is thought to be the result of myelin splitting along the intraperiod line and subsequent intramyelinic vacuolation (Soffer et al 1992). Alternatively, white matter changes may reflect cerebrovascular changes in GA-I. Non-injured patients were shown to have increased cerebral vascular volume and subsequently increased interstitial and CSF fluid volume. Therefore, T2 hyperintensity in white matter may result from increased transport of interstitial fluid from brain to CSF (Strauss et al 2010). This discrepancy may well explain why MRI white matter signals can also be found in asymptomatic GA-I patients.

In analogy to white matter changes, we identified a similar discrepancy for the globus pallidus. Although globus pallidus is an important structure of the basal ganglia and although its damage should cause an extrapyramidal syndrome, MRI changes in this nucleus, specifically T2 hyperintensities, were only weakly associated with an MD in our study. This confirms the results of a previous study (Harting et al 2009). A likely explanation for this is that globus pallidus is a myelin-rich grey matter structure (Kracun et al 1984; van der Knaap and Valk 2005) and, therefore, pallidal MRI changes may either result from acute deep grey matter injury—in combination with injury of putamen and caudate—or from chronic white matter abnormalities and/or myelination delay (Harting et al 2009). Since myelination delay is frequently observed in GA-I patients (Twomey et al 2003; Harting et al 2009), isolated pallidal MRI abnormalities may improve or even resolve along time but—in case of encephalopathic crisis—may precede pathologic signal changes of putamen and caudate. This dual role of pallidal signal changes is also shown by the fact that the globus pallidus shows an intermediate localization between putamen/caudate and white matter in the two-dimensional map.

In conclusion, this study shows that complex statistical methods such as recursive partitioning and multi-dimensional scaling are useful to decipher the age-dependent and region-specific MRI patterns of rare neurometabolic diseases such as GA-I and that these methods are helpful to elucidate the clinical relevance and prognosis of specific MRI findings. Showing collocalization of certain brain regions this study supports the hypothesis that neuroradiological abnormalities and neurological symptoms may be best explained by overlaying episodes of delayed brain maturation in utero, acute striatal injury during infancy and early childhood, and chronic extrastriatal changes that may progress lifelong.

Acknowledgments We are indebted to the patients and their families for their participation and trust. We thank the patient advocacy group "Glutarazidurie e.V." (www.glutarazidurie.de) for excellent collaboration.

This study was supported by a grant from the "Kindness for Kids" Foundation, Munich, Germany to S. K. This is a private foundation focusing on stimulating research for children with rare diseases.

Conflict of interest None.

References

Benjamini Y, Hochberg Y (1995) Controlling the false discovery rate: a practical and powerful approach to multiple testing. J R Statist Soc B 57:289–300

Bijarnia S, Wiley V, Carpenter K, Christodoulou J, Ellaway CJ, Wilcken B (2008) Glutaric aciduria type I: outcome following detection by newborn screening. J Inherit Metab Dis 31:503–507

Boneh A, Beauchamp M, Humphrey M, Watkins J, Peters H, Yaplito-Lee J (2008) Newborn screening for glutaric aciduria type I in Victoria: treatment and outcome. Mol Genet Metab 94:287–291

Busquets C, Merinero B, Christensen E et al (2000) Glutaryl-CoA dehydrogenase deficiency in Spain: evidence of two groups of patients, genetically, and biochemically distinct. Pediatr Res 48:315–322

Chow CW, Haan EA, Goodman SI et al (1988) Neuropathology in glutaric acidemia type 1. Acta Neuropathol 76:590–594

Couce ML, López-Suárez O, Bóveda MD et al (2013) Glutaric aciduria type I: outcome of patients with early- versus late-diagnosis. Eur J Paediatr Neurol 74:383–389

Funk CB, Prasad AN, Frosk P et al (2005) Neuropathological, biochemical, and molecular findings in a glutaric acidemia type 1 cohort. Brain 128:711–722

Gerstner B, Gratopp A, Marcinkowski M, Sifringer M, Obladen M, Buhrer C (2005) Glutaric acid and its metabolites cause apoptosis in immature oligodendrocytes: a novel mechanism of white matter degeneration in glutaryl-CoA dehydrogenase deficiency. Pediatr Res 57:771–776

Gitiaux C, Roze E, Kinugawa K et al (2008) Spectrum of movement disorders associated with glutaric aciduria type 1: a study of 16 patients. Mov Disord 23:2392–2397

Goodman SI, Markey SP, Moe PG, Miles BS, Teng CC (1975) Glutaric aciduria: a "new" disorder of amino acid metabolism. Biochem Med 12:12–21

Harting I, Neumaier-Probst E, Seitz A et al (2009) Dynamic changes of striatal and extrastriatal abnormalities in glutaric aciduria type I. Brain 132:1764–1782

Heringer J, Boy SPN, Ensenauer R et al (2010) Use of guidelines improves the neurological outcome in glutaric aciduria type I. Ann Neurol 68:743–752

Hothorn T, Hornik K, Zeileis A (2006) Unbiased recursive partitioning: a conditional inference framework. J Comput Graph Stat 15:651–674

Janos AL, Grange DK, Steiner RD, White DA (2012) Processing speed and executive abilities in children with phenylketonuria. Neuropsychology 26:735–743

Kölker S, Sauer SW, Surtees RA, Leonard JV (2006a) The aetiology of neurological complications of organic acidaemias—a role for the blood–brain barrier. J Inherit Metab Dis 29:701–704

Kölker S, Garbade SF, Greenberg CR et al (2006b) Natural history, outcome and therapeutic efficacy in children and adults with glutaryl-CoA dehydrogenase deficiency. Pediatr Res 59:840–847

Kölker S, Garbade SF, Boy N et al (2007) Decline of acute encephalopathic crises in children with glutaryl-CoA dehydrogenase deficiency identified by newborn screening in Germany. Pediatr Res 62:357–363

Kölker S, Christensen E, Leonard JV et al (2011) Diagnosis and management of glutaric aciduria type I—revised recommendations. J Inherit Metab Dis 34:677–694

Kracun I, Rösner H, Cosovic C, Stavljenic A (1984) Topographical atlas of the gangliosides of the adult human brain. J Neurochem 43:979–989

Külkens S, Harting I, Sauer S et al (2005) Late-onset neurologic disease in glutaryl-CoA dehydrogenase deficiency. Neurology 64:2142–2144

Lamp J, Keyser B, Koeller DM, Ullrich K, Braulke T, Mühlhausen C (2011) Glutaric aciduria type 1 metabolites impair the succinate

transport from astrocytes to neuronal cells. J Biol Chem 286:17777–17784

Lin SK, Hsu SG, Ho ES et al (2002) Novel mutations and prenatal sonographic findings of glutaric aciduria (type I) in two Taiwanese families. Prenat Diagn 22:725–729

Neumaier-Probst E, Harting I, Seitz A, Ding C, Kölker S (2004) Neuroradiological findings in glutaric aciduria type I (glutaryl-CoA dehydrogenase deficiency). J Inherit Metab Dis 27:869–876

Paradis E, Claude J, Strimmer K (2004) APE: analyses of phylogenetics and evolution in R language. Bioinformatics 20:289–290

Pfeil J, Listl S, Hoffmann GF, Kölker S, Lindner M, Burgard P (2013) Newborn screening by tandem mass spectrometry for glutaric aciduria type 1: a cost-effectiveness analysis. Orphanet J Rare Dis 8:167

R Development Core Team (2012) R: A language and environment for statistical computing. R Foundation for Statistical Computing, Vienna, ISBN 3-900051-07-0, URL http://www.R-project.org

Sauer SW, Okun JG, Schwab MA et al (2005) Bioenergetics in glutaryl-coenzyme A dehydrogenase deficiency, a role for glutaryl-coenzyme A. J Biol Chem 280:21830–21836

Sauer SW, Okun JG, Fricker G et al (2006) Intracerebral accumulation of glutaric and 3-hydroxyglutaric acids in glutaryl-coenzyme A dehydrogenase deficiency, a biochemical risk factor for neurodegeneration. J Neurochem 97:899–910

Sauer SW, Opp S, Mahringer A et al (2010) Glutaric aciduria type I and methylmalonic aciduria: simulation of cerebral import and export of accumulating neurotoxic dicarboxylic acids in in vitro models of the blood–brain barrier and the choroid plexus. Biochim Biophys Acta 1802:552–560

Sauer SW, Opp S, Hoffmann GF, Koeller DM, Okun JG, Kölker S (2011) Therapeutic modulation of cerebral L-lysine metabolism in a mouse model for glutaric aciduria type I. Brain 134:157–170

Soffer D, Amir N, Elpeleg ON et al (1992) Striatal degeneration and spongy myelinopathy in glutaric acidemia. J Neurol Sci 107:199–204

Strauss KA, Lazovic J, Wintermark M, Morton DH (2007) Multimodal imaging of striatal degeneration in Amish patients with glutaryl-CoA dehydrogenase deficiency. Brain 130:1905–1920

Strauss KA, Donnelly P, Wintermark M (2010) Cerebral haemodynamics in patients with glutaryl-coenzyme A dehydrogenase deficiency. Brain 133:76–92

Twomey EL, Naughten ER, Donoghue VB, Ryan S (2003) Neuroimaging findings in glutaric aciduria type 1. Pediatr Radiol 33:823–830

Van der Knaap MS, Valk J (2005) Myelination and retarded myelination. In: Van der Knaap MS, Valk J (eds) Magnetic resonance of myelination and myelin disorders, 3rd edn. Springer-Verlag, Berlin, pp 37–65

Viau K, Ernst SL, Vanzo RJ, Botto LD, Pasquali M, Longo N (2012) Glutaric acidemia type 1: outcomes before and after expanded newborn screening. Mol Genet Metab 106:430–438

Venables WN, Ripley BD (2002) Modern applied statistics with S, 4th edn. Springer, New York

Zinnanti WJ, Lazovic J, Housman C et al (2007) Mechanism of age-dependent susceptibility and novel treatment strategy in glutaric acidemia type I. J Clin Invest 117:3258–3270

Zschocke J, Quak E, Guldberg P, Hoffmann GF (2000) Mutation analysis in glutaric aciduria type I. J Med Genet 37:177–181